# CrystEngComm

Accepted Manuscript






ROYAL SOCIETY OF CHEMISTRY

www.rsc.org/crystengcomm

Cite this: DOI: 10.1039/c0xx00000x

www.rsc.org/xxxxxx

ARTICLE TYPE

# Single-crystal $PbTiO_3/PbZrO_3$ composite fibers formed by diffusion and epitaxial growth

**Tingting Yu, Zhaohui Ren*, Shan Jiang, Siyu Gong, Ming Li, Xiao Wei, Ge Shen, Gaorong Han***

***Received (in XXX, XXX) Xth XXXXXXXXX 20XX, Accepted Xth XXXXXXXXX 20XX***

**DOI: 10.1039/b000000x**

In this work, ferroelectric/antiferroelectric heterostructured $PbTiO_3/PbZrO_3$ composite fibers were fabricated via hydrothermal method. Single-crystal perovskite tetragonal $PbTiO_3$ (PT) nanofibers were employed as growing core to react with $PbZrO_3$ (PZ) precursors under hydrothermal conditions. Structural characterization indicated that the composite fiber consisted of single-crystal PT and PZ phases. Moreover, an epitaxial growth between the PT nanofiber and PZ crystal was revealed to occur at $(0\bar{1}1)_{PT}/(221)_{PZ}$. At the interface, $Zr^{4+}$ ions have been determined to diffuse into the nanofiber within ~20 nm and possibly substitute partial $Ti^{4+}$ positions in perovskite PT. Based on all the findings, it is proposed that the single-crystal PZ crystals on the nanofibers possibly formed via a diffusion and then epitaxial growth process under hydrothermal condition. These PT/PZ composite fibers may offer an opportunity to explore fascinating properties including dielectricity and ferroelectricity at ferroelectric/antiferroelectric interface.

## Introduction

Perovskite-structured lead titanate ($PbTiO_3$, PT), as a prototypical ferroelectric with a high Curie temperature of 490 °C, is a promising ferroelectric and piezoelectric material beacause of its large spontaneous polarization[1]. PT is also the end member of $PbZrO_3$-$PbTiO_3$ (PZT), $Pb(Mg_{1/3}Nb_{2/3})O_3$-$PbTiO_3$ (PMN-PT) and $Pb(Zn_{1/3}Nb_{2/3})O_3$-$PbTiO_3$ (PZN-PT), which have been widely applied in modern piezoelectric devices[2-5]. With the minimization of these devices, PT-based nanostructures have been intensively investigated[6-9], which are desirable objects to understand ferroelectricity and piezoelectricicty at nanoscale. In the past few years, various single-crystal PT nanostructures, including nanodots[10], nanofibers[11] and nanoplates[12], were synthesized successfully. In particular, different interfaces between these PT nanostructures and other components have been designed and prepared for realizing optimized or additional functionality. For example, single-crystal PT nanofiber-$CoFe_2O_4$ nanodot composites demonstrated ferroelectricity and ferromagnetism as well as their strong coupling at room temperature[13]. Previous work encourages us to consider whether it is possible to prepare the interface between PT and PZ because they are basic components of PZT solid solution. On the other hand, $PbTiO_3$/ $PbZrO_3$ (PT/PZ) superlattice was reported to show interesting property. For example, it is demonstrated that the dielectric constant at the stacking period of 1 unit-cell PT/1 unit-cell PZ was larger than that of single PZT solid solution film[14-17]. Such phenomenon might be caused by the interplayer stress and/or the interaction of electric dipoles between ferroelectric PT and antiferroelectric PZ layer[17]. Therefore, it is highly attactive to explore PT/PZ heterostructure with promising properties.

Despite of many efforts, there is still an absence of a simple wet-chemistry method to prepare single-crystal PT/PZ heterostructure. In our previous work, single-crystal pre-perovskite PT nanofibers were synthesized by polymer-assisted hydrothermal reaction, which could transform to single-crystal perovskite PT nanofibers via annealing treatment[11, 18]. In this work, single-crystal perovskite PT nanofibers were designed as growing core to react with PZ precursors. Then the single-crystal PZ crystals enveloped the inside PT nanofibers to form PT/ PZ composite fibers during the hydrothermal reaction. Single-crystal PZ crystals could be formed in a short hydrothermal reaction time, and an epitaxial growth relation between PT and PZ has been determined. In particular, PZ crystals could not be synthesized without the presence of PT nanofibers under the similar hydrothermal conditions. The growth of such heterostructure can be discussed by a mechanism including diffusion and epitaxial growth.

## Experimental details

**Synthesis:** Single-crystal pre-perovskite $PbTiO_3$ (PT) nanofibers were synthesized by a polymer-assisted hydrothermal method and transformed to single-crystal perovskite PT nanofibers by annealing treatment in air. These experiments details shown in Fig.1 (a) have been reported in our previous work[11]. The synthesized PT nanofibers were used as the raw material to prepare $PbTiO_3/PbZrO_3$ (PT/PZ) composite fibers by the hydrothermal method. $ZrOCl_2{\cdot}8H_2O$ (5.2 mmol), $Pb(NO_3)_2$ (10 mmol) and KOH (5 mol/L) were dissolved in deionized water. Subsequently, $ZrOCl_2{\cdot}8H_2O$, $Pb(NO_3)_2$ and KOH aqueous solution were mixed with PT nanofibers. The amount of PT nanofibers was adjusted as 3 mmol, 5 mmol and 7 mmol. After

stirring for 1 h, the resulting precursor suspension was moved into a 50 ml stainless-steel Teflon autoclave for the hydrothermal reaction at 160 °C for 4 h. Finally, it was cooled down to room temperature naturally. Then the resultant was filtered and washed for several times using deionized water and ethanol, in order to remove impurity, organic molecules and so on. Finally, the products could be obtained after being air-dried at 80 °C for 12 h (Fig.1 (b)).

**Characterization:** Powder X-ray diffraction (XRD) pattern was collected on a Thermo ARL X'TRA powder diffractometer with Bragg-Brentano geometry by Cu Kα radiation ( λ = 1.54056 Å) with 0.82 Å resolution at room temperature without any pretreatment. Raman spectra were acquired using a 100× objective on a Renishaw InVia Raman microscope equipped with an ultra-low noise charge-coupled device (CCD) detector at room temperature. The 532 nm line of a laser was used as excitation with the maximum laser power available of 50 mW and the laser power at the sample could be adjusted by opening or closing an iris shutter. All data acquisition and processing were carried out using the WiRE 3.0 software package supplied by Renishaw. The thermal analyses were determined by a SDT Q600 (TA Instruments, U.S.A) under air atmosphere and $N_2$ atmosphere at a heating rate of 10 °C/min from room temperature to 800 °C. The microstructure characteristics of the prepared samples were detected by a Hitachi field-emission scanning electron microscopy (SEM) instrument Model S-4800 at 5 kV. Transmission electron microscope (TEM) images and high-resolution TEM (HRTEM) images were taken via a transmission electron microscope (JEOL-2010) with an accelerating voltage of 200 kV, which equipped with an energy dispersive spectroscopy (EDS) detector.

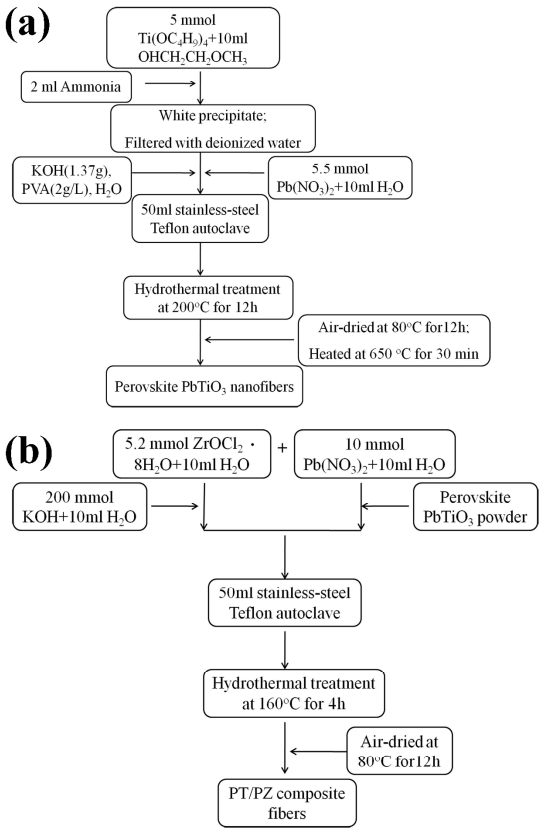


Fig.1 The flowchart for the synthesis of PT/PZ composite fibers

## Results and discussion

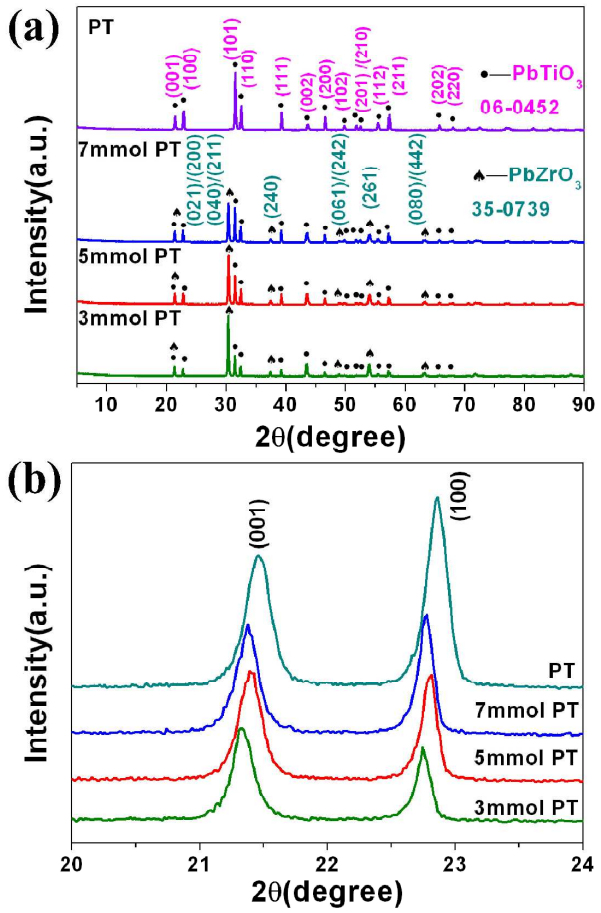


Fig.2 (a) XRD patterns of PT/PZ composite fibers, with 3 mmol, 5 mmol and 7 mmol PT nanofibers as the growing core. The uppermost curve represents the XRD pattern of pure perovskite PT nanofibers; (b) The partial XRD patterns between 20 ° and 24 °.

XRD patterns of the as-prepared PT/PZ composite fibers and pure perovskite PT nanofibers samples are shown in Fig. 2 (a). All diffraction peaks of PT/PZ composite fibers can be indexed as perovskite PT (JCPDS: 06-0452) and orthorhombic PZ (JCPDS: 35-0739). No impurity phase peak is observed. With the content of PT nanofibers increasing, the intensity of perovskite PT diffraction peaks increases, where the intensity of PZ diffraction peaks decreases. Partial XRD patterns between 20 ° and 24 ° from Fig.2 (a) are presented in Fig.2 (b). (001) and (100) peaks corresponding to PT/PZ composite fibers shift towards lower 2θ angle compared to those of pure PT nanofibers, implying an increase in the lattice parameter of PT nanofibers. The unit cell parameters derived from the XRD patterns using the Rietveld refinement method. Tab.1 shows the corresponding lattice parameters (*a* and *c*) of PT nanofibers in PT/PZ composite fibers. Compared to the lattice parameters of pure PT nanofibers, those of PT nanofibers in PT/PZ composite fibers became larger. By considering the sequence of Shannon effective ionic radii (i.e., $r(Ti^{4+}$ 60.5 pm VI)<$r(Zr^{4+}$ 72 pm VI)<$r(Pb^{2+}$ 149 pm XII)[19], the substitution of $Zr^{4+}$ ions for $Ti^{4+}$ ions at B site might cause an expansion of crystal lattices of PT structure in PT/PZ composite fibers and hence the peaks shift towards the lower 2θ angle.

Tab.1 Corresponding lattice parameters (*a* and *c*) of PT nanofibers in PT/PZ composite fibers.

| Lattice Parameters of PT nanofibers | *a* | *b* | *c* | *c/a* |
|---|---|---|---|---|
| 3 mmol-PT/PZ composite fibers | 3.901(8) | 3.901(8) | 4.151(7) | 1.0640 |
| 5 mmol-PT/PZ composite fibers | 3.900(4) | 3.900(4) | 4.148(3) | 1.0636 |
| 7 mmol-PT/PZ composite fibers | 3.902(1) | 3.902(1) | 4.152(3) | 1.0641 |
| Pure perovskite PT nanofibers | 3.895(9) | 3.895(9) | 4.148(0) | 1.0647 |

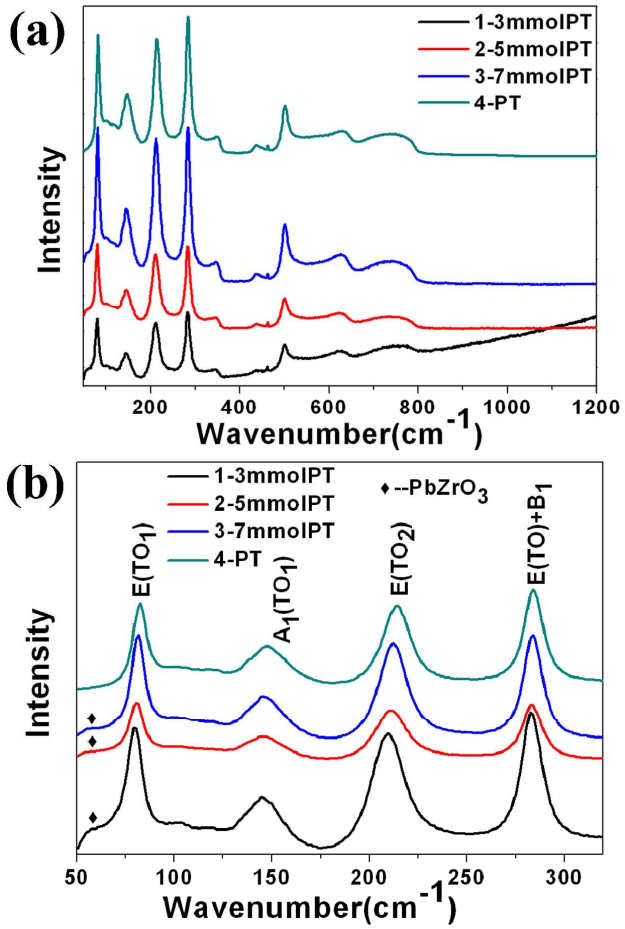


Fig.3 (a) Room-temperature Raman spectra acquired for PT/PZ composite fibers and perovskite PT nanofibers; (b) The partial Raman spectra between 50 and 350 $cm^{-1}$.

Fig.3 (a) shows the room temperature Raman spectra of PT/PZ composite fibers and perovskite PT nanofibers, within the frequency range of 50-1200 $cm^{-1}$. All the Raman modes of samples are consistent with perovskite PT nanofibers and PZ crystals[20-22]. The partial Raman spectra including $E(TO_1)$, $A_1(TO_1)$, $E(TO_2)$ and $E(TO)+B_1$ Raman modes are presented in Fig.3 (b). All the Raman modes of PT nanofibers shift towards lower wave numbers from PT nanofibers to 3 mmol-PT/PZ composite fibers, especially for $E(TO_1)$ and $E(TO_2)$ modes. The

shift of the peak position towards lower wave number in the Raman spectra are mainly caused by the decrease of tetragonality[23, 24]. According to Tab. 1, the tetragonality *c/a* of PT nanofibers in PT/PZ composite fibers is smaller than that of pure perovskite PT nanofibers. Combined with XRD results, it is assumed that the substitution of $Zr^{4+}$ ions for $Ti^{4+}$ ions gave rise to the reduced tetragonal distortion of perovskite PT nanofibers.

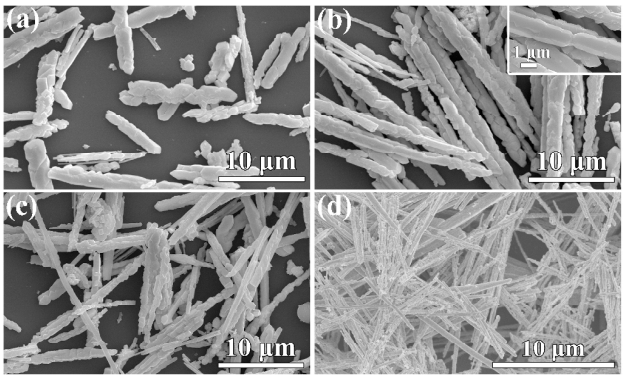


Fig.4 SEM images of PT/PZ composite fibers and perovskite PT nanofibers, (a): 3 mmol-PT/PZ; (b): 5 mmol-PT/PZ; (c): 7 mmol-PT/PZ; (d): pure perovskite PT nanofibers.

The morphology of PT/PZ composite fibers and perovskite PT nanofibers is displayed by SEM images of Fig.4. The average size of PT nanofibers derived from the SEM results (Fig.4 (d)) is around 200 nm in diameter and a few to tens micrometers in length. The irregular PZ crystals enveloped the PT nanofibers and became a smooth coating outside the PT nanofibers during the hydrothermal reaction. In general, the PT/PZ composite fibers have a length of 15-65 μm and a diameter of 0.70-2.05 μm (Fig.4 (a-c)). In addition, the amount of PT nanofibers should be appropriate to prepare samples. Otherwise, there is excessive coverage (Fig.4 (a)) or incomplete coverage (Fig.4 (c)). As displaced in Fig.4 (b), the PT nanofibers were uniformly coated by PZ crystals with appropriate amount of PT nanofibers. Besides, it is interesting to find that PZ crystals cannot be synthesized without an introduction of perovskite PT nanofibers under similar hydrothermal conditions.

In order to investigate the interface between PT and PZ, the cross section of 5 mmol-PT/PZ composite fibers were performed by resin-embedded technology. Fig. 5 (a) presents a typical TEM image of cross-section of PT/PZ composite fibers. It can be seen that PZ crystals grew around the PT nanofiber, and PZ crystals are easily broken into fractions during the sample preparation due to its brittleness. Conventional HRTEM is a very efficient method for studying the structure properties of crystals at nanoscale. HRTEM image collected from the area marked with a purple rectangle in Fig.5 (a) exhibits lattice fringes of PZ and PT. The image in Fig.5 (b) also shows a clear and simple interface with an ideal match of lattice image. The observed interplanar spacings in the area 1 are 0.279 nm, 0.282 nm and 0.285 nm, which are indexed into (110), (0$\bar{1}$1) and (101) planes of PT (JCPDS: 06-0452), respectively. The 0.410 nm, 0.418 nm and 0.291 nm intervals of the lattice fringes observed in the area 2 agree well with the spacing of the (200), (021) and (221) planes of PZ (JCPDS: 35-0739), respectively. Meanwhile, the lattice fringe of (0$\bar{1}$1) in PT matches quite well with the lattice fringe of (221) in PZ, which shows clearly at the interface of PT and PZ. The mismatch degree between PT (0$\bar{1}$1) (d=0.282 nm) and PZ (221) (d=0.291 nm) is about 3.09%, suggesting an epitaxial growth between them. The corresponding diffraction pattern of area 1 in Fig.5 (b) obtained by fast Fourier transform (FFT) indicates that the perovskite PT nanofibers are well single-crystal in nature along the [$\bar{1}$11] zone axis. The FFT pattern of area 2 in Fig.5 (b) confirms the single-crystal character of PZ crystals along the [0$\bar{1}$2] zone axis.

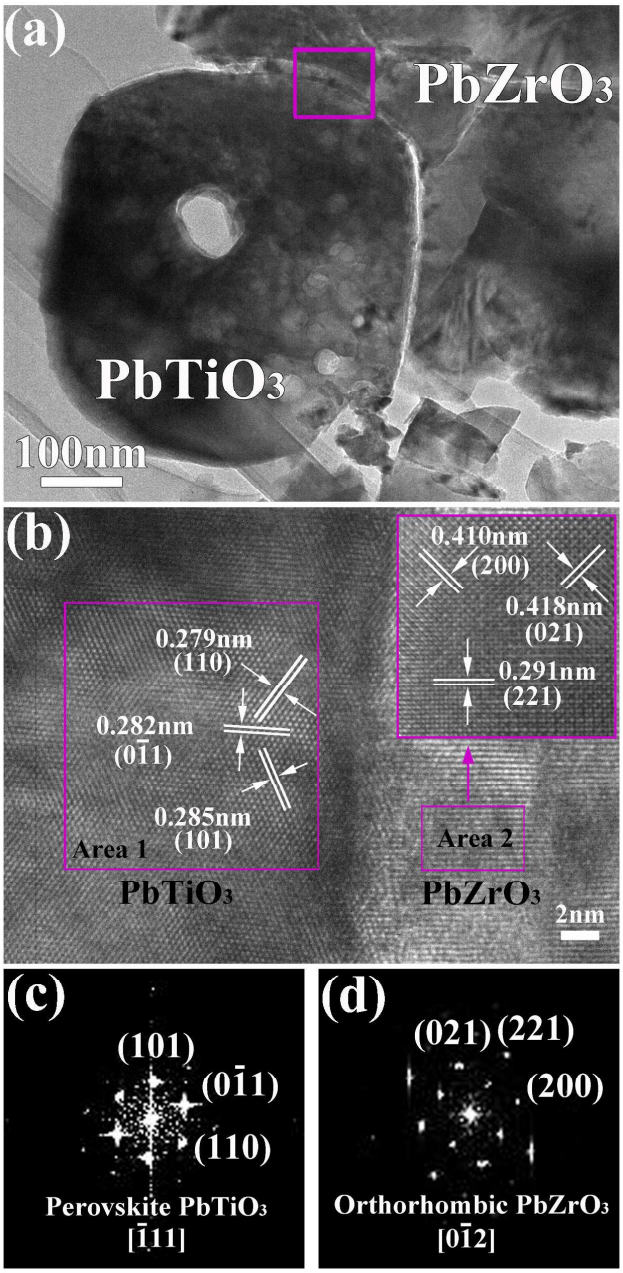


Fig.5 (a) A typical TEM image of cross-section of PT/PZ composite fibers; (b) HRTEM image collected from the area marked with a purple rectangle in Fig.5 (a); (c) FFT pattern corresponding to area 1 in Fig.5 (b); (d) FFT pattern of area 2 in Fig.5 (b).

EDS spectra in Fig.6 (b) indicates element distribution along

the purple line in Fig.6 (a), confirming that the left one is PT nanofiber and the right one is PZ crystal. According to the result of element distribution analysis, there is a clear transition area between PT nanofiber and PZ crystal. This corresponds to an interface between two phases, which is highlighted by two orange dotted lines. The width of the coexistence of Ti and Zr elements is about 10 nm, implying an interdiffusion of the atoms at the interface. Meanwhile, the range of pure PZ crystal is wider than it should be in the Fig.6 (b), compared to the length of purple line in Fig.6 (a).

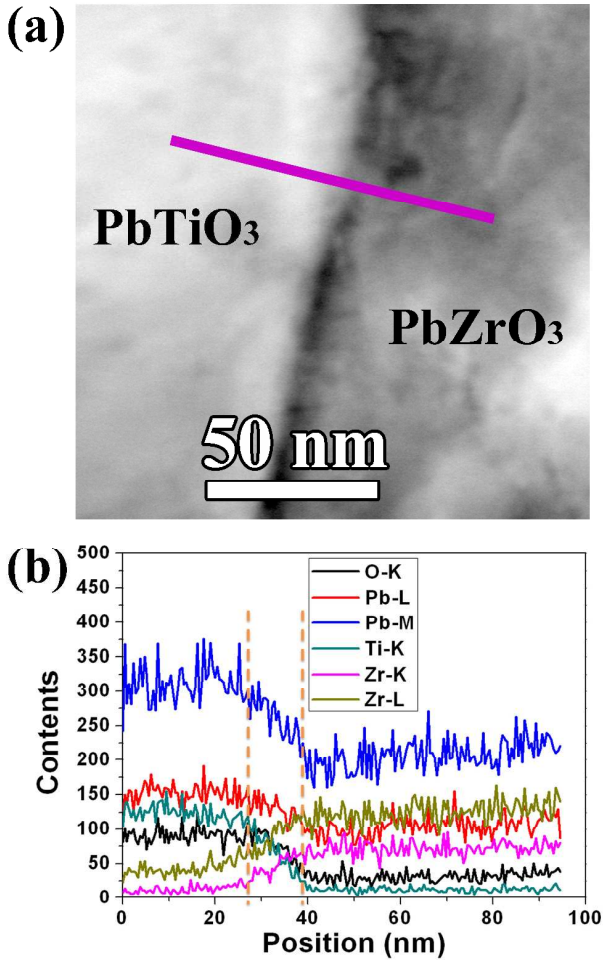


Fig.6 (a) HADDF STEM image of PT/PZ composite fibers; (b) EDS element analysis along the purple line in Fig.6 (a).

Fig.7 (b-e) list the elements distribution collected from the area marked with a purple rectangle in the HADDF STEM image of PT/PZ composite fibers shown in Fig.7 (a). As expected, Pb and O elements are almost uniformly distributed according to Fig.7 (b-c). In particular, Zr and Ti element distributions both have a sharp dividing line. The interface is not the boundary of Zr and Ti elements and the real dividing line could be emphasized in Fig.7 (a) using dark color on the basis of Fig.7 (d-e). Besides, it can be seen that Zr and Ti elements coexist around the dividing line, which is also confirmed by the EDS element analysis (Fig.6 (b)).

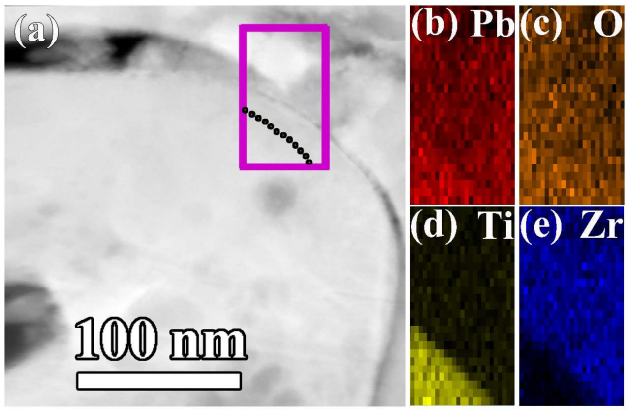


Fig.7 (a) HADDF STEM image of PT/PZ composite fibers; (b-e) Elements distribution collected from the area marked with a purple rectangle in Fig.7 (a): (b) Pb; (c) O; (d) Ti; (e) Zr.

As discussed in solid state reactions of $PbTiO_3$-$PbZrO_3$ system[23-25], PT phase was formed initially and then the interdiffusion of $Ti^{4+}$ and $Zr^{4+}$ resulted in an overall formation of a homogeneous PZT solid solution. Saburo et al.[26] discussed a two-step process for PZT formation. In the first step, a PT phase was formed. In the second step, the occurrence of highly activated Zr ions and PZ (in a nucleation state) played an important role in the formation of PZT solid solution. In our study, the similar process is that PT phase was prepared firstly. For the formation of the single-crystal PZ with the presence of PT nanofibers, it is proposed that partial $Zr^{4+}$ ions firstly diffused into PT nanofibers and the interface between PT nanofiber and PZ crystal was clearly visible in Fig.5. However, no PZT solid solution was formed. In order to explain the growth mechanism of single-crystal PT/PZ composite fibers, the following work has been done.

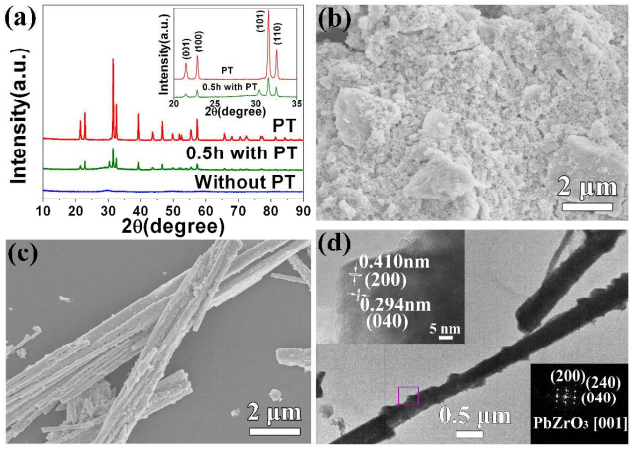


Fig.8 (a) XRD patterns of samples prepared without PT nanofibers, PT/PZ composite fibers after 0.5 h hydrothermal reaction and pure perovskite PT nanofibers; The inset shows the enlarged (001), (100), (101) and (110) diffraction peaks for the XRD pattern; (b) SEM image of amorphous particles prepared without PT nanofibers; (c) SEM image of PT/PZ composite fibers after 0.5 h hydrothermal reaction; (d) A typical TEM image of PT/PZ composite fibers after 0.5 h hydrothermal reaction, the upper-left inset is HRTEM image of PZ crystals collected from the area marked with a purple rectangle, the bottom-right inset is corresponding FFT pattern along [001] zone axis.

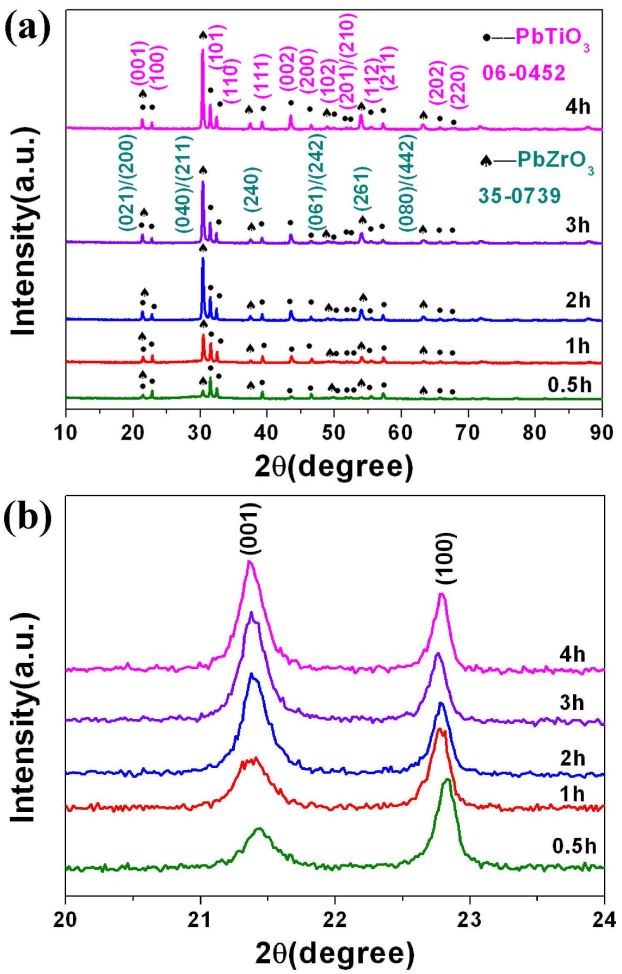


Fig.9 (a) XRD patterns of PT/PZ composite fibers for different hydrothermal reaction time; (b) The enlarged (001) and (100) diffraction peaks for the XRD pattern.

As demonstrated by XRD (Fig.8 (a)) and SEM (Fig.8 (b)) results, PZ crystals could not be synthesized without the presence of PT nanofibers under similar hydrothermal conditions. It is reasonable to consider that the introduction of PT nanofibers possibly decreased PZ nucleation potential barrier and then PZ crystals nucleated and grew on the surface of PT nanofibers. In particular, PZ crystals have already been formed after a hydrothermal reaction for 0.5 h with an introduction of PT nanofibers (Fig.8 (a)). Compared to pure PT diffraction peaks, the enlarged (001), (100), (101) and (110) peaks of the sample after 0.5 h hydrothermal reaction shift towards lower 2θ angle, shown in the inset of Fig.8 (a). It is suggested that $Zr^{4+}$ ions with larger radius could replace $Ti^{4+}$ positions of PT nanofibers in such a short time. Fig.8 (c) illustrates the SEM image of PT/PZ composite fibers after 0.5 h hydrothermal reaction. PT nanofibers were coated by a PZ thin layer, representing the formation of PT/PZ composite fibers. A typical TEM image of PT/PZ composite fibers after 0.5 h hydrothermal reaction is presented in Fig.8 (d). The upper-left inset is HRTEM image of PZ crystals collected from the area marked with a purple rectangle. The interplanar spacings are 0.410 nm and 0.294 nm, which can be indexed into (200) and (040) planes of PZ (JCPDS: 35-0739), respectively. The FFT pattern in the bottom-right inset confirms the single-crystal character of PZ crystals along the [001] zone axis. The results in Fig.8 lead us to consider that the diffusion of $Zr^{4+}$ ions and the growth of PZ crystals are very fast, which proceed simultaneously. This can be supported by XRD pattern in Fig.9. As shown in Fig.9 (a), with extending the hydrothermal reaction time from 0.5 h to 4 h, the intensity of PZ peaks increases accordingly, indicating the enhancement of crystallinity. In particular, all the peaks of PT phase, such as (001) and (100) peaks in Fig.9 (b), shift towards lower 2θ angle. The increase in the lattice parameter of PT nanofibers arises from the replacement of $Ti^{4+}$ ions by $Zr^{4+}$ ions. High concentration of $Zr^{4+}$ ions in the solution can lead to the diffusion of $Zr^{4+}$ ions into the structure of PT nanofiber and replacing $Ti^{4+}$ positions. The replacement distance of ~20 nm wide was found in Fig.7.

According to the above results, the diffusion of $Zr^{4+}$ ions and the growth of PZ crystals proceeded simultaneously during the growth of single-crystal PT/PZ composite fibers, which cannot be simply explained by heterogeneous nucleation or homogeneous nucleation. Therefore, a schematic diagram is provided to illustrate the growth mechanism of PT/PZ composite fibers, as displayed in Fig.10. Fig.10 (a) shows the perovskite PT nanofibers used as growing core to prepare PT/PZ composite fibers. The activated $Zr^{4+}$ ions diffused into the structure of PT nanofiber to replace $Ti^{4+}$ positions, thus about 20 nm single-crystal PZ layer formed under the hydrothermal conditions (Fig.10 (b)), confirmed by Fig.7. Proceeding with hydrothermal reaction, $Zr^{4+}$ and $Pb^{2+}$ ions deposited on the surface of the emerged single-crystal PZ thin layer and epitaxially grew to form large PZ crystals around the PT nanofibers. It is reasonable to expect that the diffusion and subsequent epitaxial growth lead to a quick crystal growth of PZ crystals. This can explain why single-crystal PZ crystals can be synthesized only after a short hydrothermal reaction time (0.5 h). Besides, the uneven coverage of PZ crystals around PT nanofibers may result from the inhomogeneous diffusion. With the hydrothermal reaction time increasing, PZ crystals become a more smooth coating that enveloped PT nanofibers.

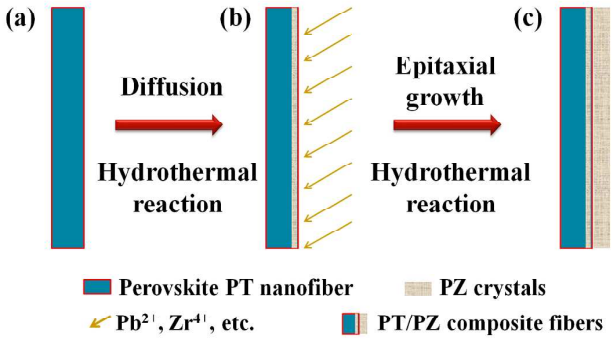


Fig.10 Schematic illustration of the growth mechanism for PT/PZ composite fibers

## Conclusions

In summary, single-crystal PT/PZ composite fibers were synthesized by hydrothermal method for the first time. Structural characterization indicated that PT and PZ phases were both single-crystal. Moreover, the findings demonstrated an epitaxial growth relation between the PT nanofibers and PZ crystals

occurred at $(011)_{PT}/(221)_{PZ}$. The growth mechanism including diffusion and epitaxial growth was proposed to explain the growth of PT/PZ heterostructure. It is demonstrated that the diffusion of $Zr^{4+}$ ions and the growth of PZ crystals proceeded fast and simultaneously. Such ferroelectric/antiferroelectric PT/PZ heterostructure may offer an opportunity to explore interesting properties including ferroelectric and dielectric properties.

## Acknowledgement

This work was financially supported by the National Nature Science Foundation of China (No.51102212) and (No.51232006).

## Notes and references

*State Key Lab of Silicon Materials, Department of Material Science and Engineering and Cyrus Tang Center for Sensor Materials and Applications, Zhejiang University, Hangzhou 310027, PR China*
**Corresponding author: E-mail: renzh@zju.edu.cn*
*Tel: +86-571-87951649; Fax: +86-571-87952341*
*Email: hgr@zju.edu.cn*
*Tel:+86-571-87951649; Fax:+86-571-87952341*

1 R. E. Cohen, *Nature*, 1992, **358**, 136-138.
2 G. Sebald, L. Seveyrat, D. Guyomar, L. Lebrun, B. Guiffard and S. Pruvost, *J. Appl. Phys.,* 2006, **100**, 124112.
3 Z. G. Wu and R. E. Cohen, *Phys. Rev. Lett.*, 2005, **95**, 037601.
4 S. E. Park and T. R. Shrout, *J. Appl. Phys.,* 1997, **82**, 1804-1811.
5 U. Belegundu, X. H. Du, A. Bhalla and K. Uchino, *Ferroelectrics Lett.*, 1999, **26**, 107-116.
6 S. Xu, B. J. Hansen and Z. L. Wang, *Nat. Commun.*, 2010, **1**. Article number: 93.
7 Z. H. Ren, G. Xu, X. Wei, Y. Liu, G. Shen and G. R. Han, *J. Am. Ceram. Soc.*, 2007, **90**, 2645-2648.
8 Z. Xiao, Z. H. Ren, Z. Y. Liu, X. A. Wei, G. Xu, Y. Liu, X. A. Li, G. Shen and G. R. Han, *J. Mater. Chem.*, 2011, **21**, 3562-3564.
9 X. Chen, S. Y. Xu, N. Yao and Y. Shi, *Nano. Lett.*, 2010, **10**, 2133-2137.
10 S. Yin, H. Tian, Z. Ren, X. Wei, C. Chao, J. Pei, X. Li, G. Xu, G. Shen and G. Han, *Chem. Comm.*, 2014, **50**, 6027-6030.
11 Z. Y. Liu, Z. H. Ren, Z. Xiao, C. Y. Chao, X. Wei, Y. Liu, X. Li, G. Xu, G. Shen and G. R. Han, *Small*, 2012, **8**, 2959-2963.
12 C. Y. Chao, Z. H. Ren, Y. H. Zhu, Z. Xiao, Z. Y. Liu, G. Xu, J. Q. Mai, X. Li, G. Shen and G. R. Han, *Angew. Chem. Int. Edit.*, 2012, **51**, 9283-9287.
13 Z. H. Ren, Z. Xiao, S. M. Yin, J. Q. Mai, Z. Y. Liu, G. Xu, X. Li, G. Shen and G. R. Han, *J. Alloy. Compd.*, 2013, **552**, 518-523.
14 T. Choi and J. Lee, *Ferroelectrics*, 2005, **328**, 41-46.
15 J. L. Blok, D. H. A. Blank, G. Rijnders, K. M. Rabe and D. Vanderbilt, *Phys. Rev. B*, 2011, **84**, 205413.
16 L. Li and X. M. Chen, *Mat. Sci. Eng. B-Solid*, 2004, **108**, 200-205.
17 I. Kanno, S. Hayashi, R. Takayama and T. Hirao, *Appl. Phys. Lett.,* 1996, **68**, 328-330.
18 Z. H. Ren, G. Xu, Y. Liu, X. Wei, Y. H. Zhu, X. B. Zhang, G. L. Lv, Y. W. Wang, Y. W. Zeng, P. Y. Du, W. J. Weng, G. Shen, J. Z. Jiang and G. R. Han, *J. Am. Chem. Soc.*, 2010, **132**, 5572-5573.
19 R. D. Shannon, *Acta. Crystallogr. A*, 1976, **32**, 751-767.
20 M. D. Fontana, H. Idrissi, G. E. Kugel and K. Wojcik, *J. Phys.: Condens. Matter.*, 1991, **3**, 8695-8705.
21 G. Burns and B. A. Scott, *Phys. Rev. B*, 1973, **7**, 3088-3101.
22 A. E. Pasto and R. A. Condrate, *J. Am. Ceram. Soc.*, 1973, **56**, 436-438.
23 Y. Deng, Z. Yin, Q. Chen, M. S. Zhang and W. F. Zhang, *Mater. Sci. Eng., B,* 2001, **84**, 248-251.
24 M. D. Fontana, H. Idrissi and K. Wojcik, *Europhys. Lett.,* 1990, **11**, 419-424.
25 S. S. Chandratreya, R. M. Fulrath and J. A. Pask, *J. Am. Ceram. Soc.*, 1981, **64**, 422-425.
26 D. L. Hankey and J. V. Biggers, *J. Am. Ceram. Soc.*, 1981, **64**, C172-C173.
27 Y. Matsuo and H. Sasaki, *J .Am. Ceram. Soc.*, 1965, **48**, 289-291.
28 S. Mori, H. Mitsuda, K. Date, Y. Hiori and T. Miyazawa, *Nat.Tech. Rept. (Matsushita Elec. Ind. Co., Osaka),* 1964, **10**, 32-40.

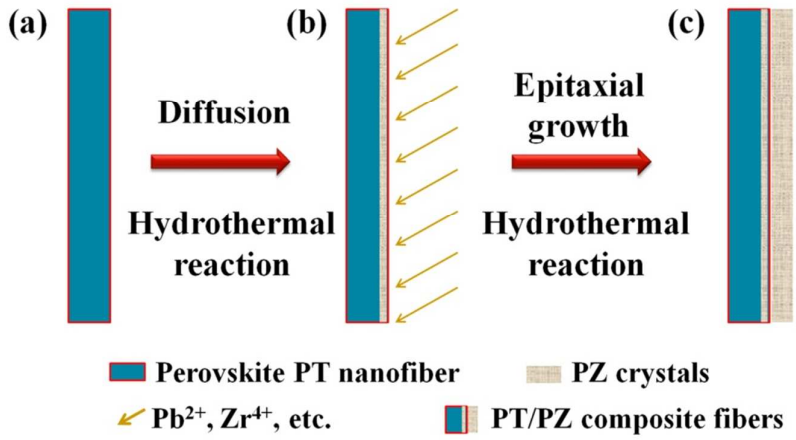


**[Highlights]**

Single-crystal $PbTiO_3/PbZrO_3$ (PT/PZ) composite fibers were prepared under hydrothermal conditions for the first time, which had an epitaxial growth relation between single-crystal perovskite PT nanofibers and PZ crystals.